IEEE Access
Multidisciplinary | Rapid Review | Open Access Journal

Received 16 March 2023, accepted 6 April 2023, date of publication 10 April 2023, date of current version 13 April 2023.

Digital Object Identifier 10.1109/ACCESS.2023.3265804

RESEARCH ARTICLE

Numerical Simulation and Equivalent Circuit Model of Multi-Band Terahertz Absorber Composed of Double-Sided Graphene Comb Resonator Array

SOMAYYEH ASGARI AND TAPIO FABRITIUS

Optoelectronics and Measurement Techniques Research Unit, Faculty of Information Technology and Electrical Engineering, University of Oulu, Oulu 90570, Finland

Corresponding author: Somayyeh Asgari (Somayyeh.asgari@oulu.fi)

This work was supported by the Academy of Finland under Grant 320017.

ABSTRACT Multi-band terahertz (THz) absorber based on a non-symmetric double-sided graphene comb resonator array is designed and simulated by the finite element method (FEM) in CST Software. Then, an equivalent circuit model (ECM) based on admittance with a fast MATLAB code is proposed to analyze the absorber in the THz region. The admittance-based ECM approach could be used for any metamaterial absorber containing one layer of resonators sandwiched between two dielectric slabs and backed by a metal layer consisting of a layer of resonators with a thickness much smaller than the minimum wavelength in the considered wavelength range. The proposed absorber is dynamically tunable with a one-layered resonator array. It has strong linear dichroism (LD) response of 98% and the frequency range of 0.7-5 THz with absorption >96%: two absorption bands for TE mode and three for TM mode. The proposed absorber can be used in polarization-sensitive devices and systems in the THz region. The ECM model of the metastructure was derived to provide an efficient approach to analyzing the performance of the absorber. The FEM simulation results are in good agreement with the ECM ones.

INDEX TERMS Terahertz metamaterials, graphene devices, electromagnetic absorber, equivalent circuit model.

I. INTRODUCTION

Metamaterials consisting of single or multi-layer of resonator arrays and having non-symmetrical geometries with the possibility to superimpose on their mirror image by the degrees of rotation have attracted broad attention for their features [1], [2], [3], [4], [5], [6]. This type of metamaterials has shown a capability to produce chirality responses such as circular dichroism (CD) [7], [8], [9], [10] or linear dichroism (LD) [10], [11], [12]. Metamaterials with non-symmetrical geometries have been designed and proposed for different applications such as absorbers [8], [12], [13], biosensors [14], [15], converters [16], [17], switches [18], [19], and mirrors [6], [20] recently showing their versatile possibilities in various the fields of science.

Graphene is an ultra-thin layer of carbon atoms with a thickness of 0.335 nm [21], [22] and it has been widely used in patterned and non-patterned forms in optoelectronic devices [23] as it can dynamically control the electromagnetic waves by the alternation of the applied external bias voltage. This distinguishes 2D materials like graphene from the other commonly used materials like metals or dielectrics. Hence it is possible to tune the output spectra of the devices containing graphene without the need to refabricate the devices saving materials, costs, and time [4], [6], [12], [17], [20], [21], [22], [23], [24] making them very interesting, especially for spectroscopic applications.

One category of graphene metamaterials is the structures with non-symmetrical geometries including graphene chiral

The associate editor coordinating the review of this manuscript and approving it for publication was Santosh Kumar.

or anisotropic metamaterials containing one or multi-layered graphene resonator array(s). They have been designed and investigated, recently showing dynamically tunable high (up to 99%) chirality responses [4], [5], [6], [12], [17], [20], [25], [26]. Thus, graphene metamaterials with strong chirality responses such as LD have recently been in the scope of interest among worldwide researchers because they can greatly increase the photon-matter interaction necessary in many sensing applications.

There are some recent reports about non-dynamically tunable single or dual-band absorbers with non-symmetrical geometries [27], [28], [29], [30], [31], [32]. In addition, dynamically tunable THz region graphene absorbers with non-symmetrical geometries containing one resonator in each unit cell with a single layer of resonators (up to three absorption bands) with high absorption have been published [12], [33]. However, for having many absorption bands and high average absorption, metamaterials containing multi-layer of resonators or super unit cells have been the most promising candidates so far [34], [35], [36]. The design of dynamically tunable multi-band absorbers with high average absorption containing a single resonator layer and one resonator in each unit cell (simple geometries) is in the scope of interest of this study. The reduction of structural complexity is expected to save material and cost resources and make their fabrication more feasible.

Graphene-based multi-band THz absorbers are potential enablers for future photonics systems. By tuning the spectral response of the metamaterial absorber, they can be utilized in multi-channel communication systems [37], highly sensitive and selective sensing and imaging, spectroscopy applications [38], [39], [40], [41], [42], [43], filtering [40], switching [42], modulating [43], and so on.

In this paper, we designed and analyzed a multi-band graphene absorber in the THz region. The absorber consists of a non-symmetric double-sided graphene comb resonator array. An admittance-based equivalent circuit model (ECM) of the metamaterial is implemented. The designed metamaterial is analyzed primarily as an absorber, but it can be used also in applications like filtering and sensing in the THz devices and systems.

II. DESIGN AND MODELING OF THE ABSORBER

Structural views of the proposed multi-band THz graphene absorber consisting of a non-symmetric double-sided comb resonator array are presented in Fig. 1. An ion gel layer is assumed to be lossless and dispersionless layer with a refractive index of 1.42 being placed over the metamaterial to bias the graphene resonator array layer [12], [44]. The resonator array layer is made of graphene which enables the device to be dynamically tunable (not possible by metals). Basically, this means that there is no need to refabricate the metamaterial for tuning it's spectral response saving the resources of materials, costs, and time [24]. The main loss and dispersion for the metamaterial are produced by the

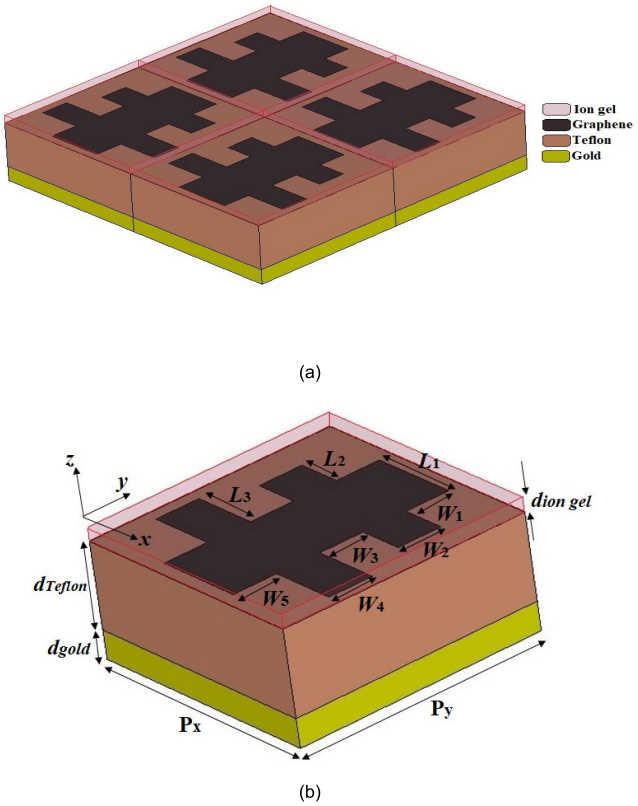

FIGURE 1. (a) Periodic and (b) unit cell views of the multi-band terahertz graphene absorber consisting of a non-symmetric double-sided comb resonator array. The ion gel layer is used to bias the graphene resonator array. The substrate is made of Teflon and the structure is backed by a gold layer to avoid the transmission of electromagnetic waves.

graphene resonator layer. The substrate is built of Teflon (polytetrafluoroethylene or PTFE) with a low permittivity of $\varepsilon_d = 2.1$ and an extremely low loss tangent ($\tan\delta = 0.0003$) which are stable over a wide range of frequencies. Teflon has unique electrical and mechanical properties. It has very small dielectric loss and it is dispersionless in the considered frequency region with high-performance thermoplastic polymer characteristics [12], [45], [46]. A layer of gold with a conductivity of 4.56×10^7 S/m [47] is used which acts as a perfect reflector in the considered frequency range. In addition, it doesn't produce any loss since it has a big conductivity and energy cannot go through it [48] and it is dispersionless. It is placed at the bottom of the metamaterial. The gold reflector with a thickness of 0.5 μm which is much larger than of the penetration depth ($\sim$5.5 $\times$ maximum penetration depth) of the THz waves is selected to ensure that the incident electromagnetic wave cannot transmit to the other side of the absorber [49]. The numerical simulation results are obtained by the finite element method (FEM) in the frequency domain of CST Software [12], [20], [33], [50], [51]. The boundary conditions and the mesh type are being considered the same as reported in [33]. The designed metamaterial works as a dynamically tunable multi-band absorber in the THz range. We swept and optimized the dimensions of the metamaterial

TABLE 1. The optimized dimensional values of the metamaterial.

Parameter	Value	Parameter	Value	Parameter	Value
L_1	10 μm	L_2	5μm	L_3	7.5 μm
W_1	5 μm	W_2	5 μm	W_3	5 μm
W_4	5 μm	W_5	5 μm	$d_{ion\ gel}$	0.15 μm
d_{Teflon}	7 μm	d_{gold}	0.5 μm	P_x	28 μm
P_y	28 μm				

absorber in the 0.7-5 THz frequency range in the CST Software to achieve the highest linear dichroism (LD) response, the maximum number of absorption bands, and the highest average absorption. The optimized dimensional values of the proposed metamaterial are reported in Table 1.

The dimensional parameters are obtained by use of the genetic algorithm optimization technique in CST. Genetic algorithms (GAs) are heuristic searches and optimization techniques inspired by natural evolution [52], [53].

In the simulated frequency range, the maximum frequency is $f_{max} = 5$ THz (minimum wavelength is $\lambda_{min} = 60\ \mu$m) and the unit cell dimensions are $P_x = P_y = 28\ \mu$m along the x and y axes which are smaller than $0.8^*\lambda_{min} = 48\ \mu$m. So, the higher-order Floquet modes will not be excited and propagated in the device [54], [55].

The μ_c, graphene chemical potential, is considered as 1 eV in the design. The relative permittivity of graphene is calculated by [33]:

$$\varepsilon = 1 - j\frac{\sigma}{\omega\varepsilon_0\Delta} \tag{1}$$

where σ, ω, ε_0, and Δ are the graphene surface conductivity, angular frequency, permittivity of vacuum, and the graphene thickness. Δ is 0.335 nm. The σ contains both inter- and intraband electron transition contributions based on the Kubo formula [12]:

$$\sigma = \sigma_{\text{inter}}(\omega) + \sigma_{\text{intra}}(\omega) \tag{2a}$$

$$\sigma_{\text{inter}}(\omega) = \frac{e^2}{4\hbar}\left[H\left(\frac{\omega}{2}\right) - \frac{4j\omega}{\pi}\int_0^\infty \frac{H(\xi) - H\left(\frac{\omega}{2}\right)}{\omega^2 - 4\xi^2}d\xi\right] \tag{2b}$$

$$\sigma_{\text{intra}}(\omega) = \frac{2k_B e^2 T}{\pi\hbar^2}\ln\left[2\cosh\left(\frac{E_f}{2k_B T}\right)\right]\frac{j}{j\tau^{-1} - \omega} \tag{2c}$$

$$H(\xi) = \frac{\sinh\left(\frac{\hbar\xi}{k_B T}\right)}{\cosh\left(\frac{E_f}{k_B T}\right) + \cosh\left(\frac{\hbar\xi}{k_B T}\right)} \tag{2d}$$

where $\hbar$ is the reduced Plank's constant, $k_B = 1.38 \times 10^{-23}$ J/K is Boltzmann's constant, $e = 1.6 \times 10^{-19}$ C is the electron charge, T is the temperature (300 K),

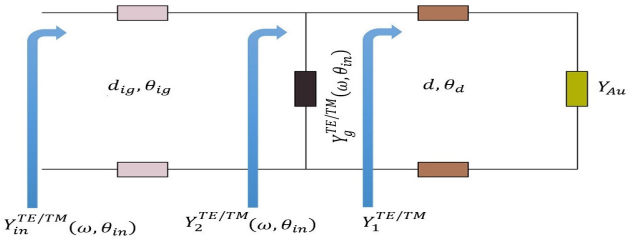

FIGURE 2. The equivalent circuit model (ECM) of the proposed graphene absorber of Fig. 1 when it is illuminated by TE/TM electromagnetic modes.

and ζ is the integral variable. τ is the relaxation time [56]:

$$\tau = \frac{\mu E_f}{e v_f^2} \tag{3}$$

where $v_f = 10^6$ m/s is the Fermi velocity and $\mu = 2.22$ m^2/(V.s) is the carrier mobility of graphene. The propagation constant of the electromagnetic wave in a graphene-vacuum configuration is [33]:

$$\beta = k_0\sqrt{1 - \left(\frac{2Y_0}{\sigma}\right)^2} \tag{4}$$

where k_0 and Y_0 are the wave vector of the incident wave and the vacuum admittance.

The equivalent circuit model (ECM) of the designed graphene absorber of Fig. 1 when it is excited by TE/TM electromagnetic modes is given in Fig. 2. The transmission line model and the input admittance for each section of the designed graphene absorber are shown in Fig. 2. The thickness of the graphene layer is much smaller than the simulated wavelength range, so the graphene resonator layer is modeled as a point load [57], [58].

The admittances of the different sections of the graphene absorber are calculated by [57]:

$$Y_1^{TE/TM} = Y_d^{TE/TM}\frac{Y_{Au} + jY_d^{TE/TM}.\tan(\beta_d d)}{Y_d^{TE/TM} + jY_{Au}.\tan(\beta_d d)} \tag{5}$$

in which $Y_d^{TE/TM}$, and β_d are respectively the TE/TM admittances of the Teflon dielectric spacer, the gold layer admittance, and the propagation constant of the TE/TM electromagnetic wave in the dielectric spacer. The admittance of the metal back layer is considered zero:

$$Z_{Au} = 0 \tag{6}$$

So, we have:

$$Y_{Au} = \frac{1}{Z_{Au}} = \infty \tag{7}$$

and

$$\lim_{Y_{Au}\to\infty} Y_1^{TE/TM} = -jY_d^{TE/TM}\cot(\beta_d d), \tag{8}$$

where

$$Y_d^{TE} = Y_0\sqrt{\varepsilon_d}\sec(\theta_d) \tag{9}$$

θ_d is the electrical length of the Teflon layer:

$$\theta_d = \frac{d\omega\sqrt{\varepsilon_d}}{c} \tag{10}$$

$$Y_d^{TM} = Y_0\sqrt{\varepsilon_d}\cos(\theta_d) \tag{11}$$

$$\beta_d = \frac{\omega\sqrt{\varepsilon_d}}{c} \tag{12}$$

So, Eq. 5 in TE mode is simplified to:

$$Y_1^{TE} = -jY_0\sqrt{\varepsilon_d}\sec(\theta_d)\cot(\beta_d d) \tag{13}$$

So, Eq. 5 in TM mode is simplified to:

$$Y_1^{TM} = -jY_0\sqrt{\varepsilon_d}\cos(\theta_d)\cot(\beta_d d) \tag{14}$$

$$Y_2^{TE/TM} = Y_g^{TE/TM} + Y_1^{TE/TM} = \frac{p_2^{TE/TM}}{q_2^{TE/TM}} \tag{15}$$

where $Y_g^{TE/TM}$ are the equivalent admittances of the graphene resonator array in TE/TM modes and they contain of both real and imaginary parts. These Eqs of the equivalent admittances are valid for any resonator layer with a thickness much smaller than the minimum wavelength (λ_{min}) in the considered wavelength range. If the resonator pattern changes, the values of the equivalent admittances will change. The equivalent admittances (conductivities) are calculated by:

$$Y_g^{TE}(\omega,\theta_{in}) = \sigma_g^{TE}(\omega,\theta_{in}) = \frac{Y_0\begin{bmatrix}\cos(\theta_{in}) - \sqrt{\varepsilon_d}\cos(\theta_{out}) \\ -r^{TE}\left(\cos(\theta_{in}) + \sqrt{\varepsilon_d}\cos(\theta_{out})\right)\end{bmatrix}}{\left(1+r^{TE}\right)} \tag{16}$$

$$Y_g^{TM}(\omega,\theta_{in}) = \sigma_g^{TM}(\omega,\theta_{in}) = \frac{Y_0\begin{bmatrix}\sec(\theta_{in}) - \sqrt{\varepsilon_d}\sec(\theta_{out}) \\ -r^{TM}\left(\sec(\theta_{in}) + \sqrt{\varepsilon_d}\sec(\theta_{out})\right)\end{bmatrix}}{\left(1+r^{TM}\right)} \tag{17}$$

where θ_{in}, θ_{out}, r^{TE}, and r^{TM} are respectively the angle of the incident launched wave, the angle of the transmitted wave, the reflection coefficient of the resonator layer in TE mode, and the reflection coefficient of the resonator layer in TM mode. r^{TE} and r^{TM} are calculated in CST when the graphene resonator array is placed on a half-space Teflon dielectric spacer with a thickness of 500 μm. If the resonator pattern changes, the values of the r^{TE} and r^{TM} will change and the values of the equivalent admittances (Eqs. 16 and 17) will change.

$$Y_2^{TE} = \frac{\begin{bmatrix}Y_0^2\cos(\theta_{in}) - Y_0^2\sqrt{\varepsilon_d}\cos(\theta_{out}) \\ -Y_0^2 r^{TE}\left(\cos(\theta_{in}) + \sqrt{\varepsilon_d}\cos(\theta_{out})\right) \\ -j\left(1+r^{TE}\right)\sqrt{\varepsilon_d}\sec(\theta_d)\cot(\beta_d d)\end{bmatrix}}{Y_0\left(1+r^{TE}\right)} \tag{18}$$

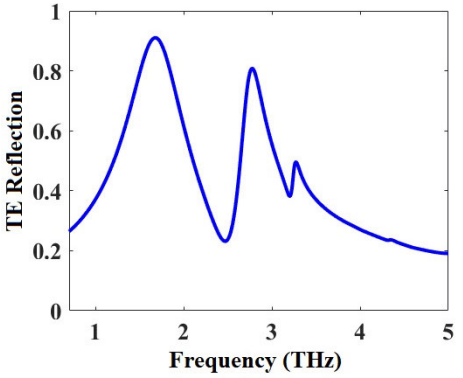

(a)

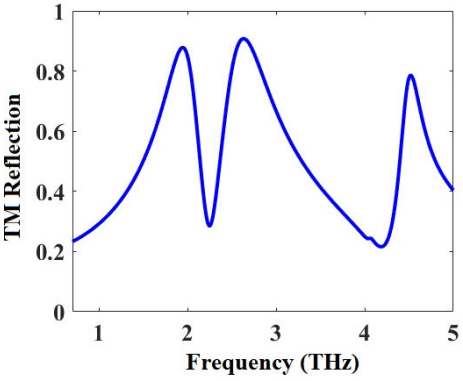

(b)

FIGURE 3. (a) TE and (b) TM reflection spectra of the graphene resonator array layer when it is placed over a Teflon dielectric layer as a half-space dielectric layer with a thickness of 500 μm.

based on Eqs. 15 and 18:

$$p_2^{TE} = \begin{bmatrix}Y_0^2\cos(\theta_{in}) - Y_0^2\sqrt{\varepsilon_d}\cos(\theta_{out}) \\ -Y_0^2 r^{TE}\left(\cos(\theta_{in}) + \sqrt{\varepsilon_d}\cos(\theta_{out})\right) \\ -j\left(1+r^{TE}\right)\sqrt{\varepsilon_d}\sec(\theta_d)\cot(\beta_d d)\end{bmatrix} \tag{19}$$

$$Y_2^{TM} = \frac{\begin{bmatrix}Y_0^2\sec(\theta_{in}) - Y_0^2\sqrt{\varepsilon_d}\sec(\theta_{out}) \\ -Y_0^2 r^{TM}\left(\sec(\theta_{in}) + \sqrt{\varepsilon_d}\sec(\theta_{out})\right) \\ -j\left(1+r^{TM}\right)\sqrt{\varepsilon_d}\cos(\theta_d)\cot(\beta_d d)\end{bmatrix}}{Y_0\left(1+r^{TM}\right)} \tag{20}$$

based on Eqs. 15 and 20:

$$p_2^{TM} = \begin{bmatrix}Y_0^2\sec(\theta_{in}) - Y_0^2\sqrt{\varepsilon_d}\sec(\theta_{out}) \\ -Y_0^2 r^{TM}\left(\sec(\theta_{in}) + \sqrt{\varepsilon_d}\sec(\theta_{out})\right) \\ -j\left(1+r^{TM}\right)\sqrt{\varepsilon_d}\cos(\theta_d)\cot(\beta_d d)\end{bmatrix} \tag{21}$$

The input admittances in TE/TM modes of the whole absorber are calculated by:

$$Y_{in}^{TE/TM} = Y_{ig}^{TE/TM}\frac{Y_2^{TE/TM} + jY_{ig}^{TE/TM}.\tan\left(\beta_{d_{ig}}d_{ig}\right)}{Y_{ig}^{TE/TM} + jY_2^{TE/TM}.\tan\left(\beta_{d_{ig}}d_{ig}\right)} \tag{22}$$

where $Y_d^{TE/TM}$ and β_d are respectively the TE/TM admittances of the ion gel dielectric and the propagation constant of the TE/TM electromagnetic wave in the ion gel dielectric.

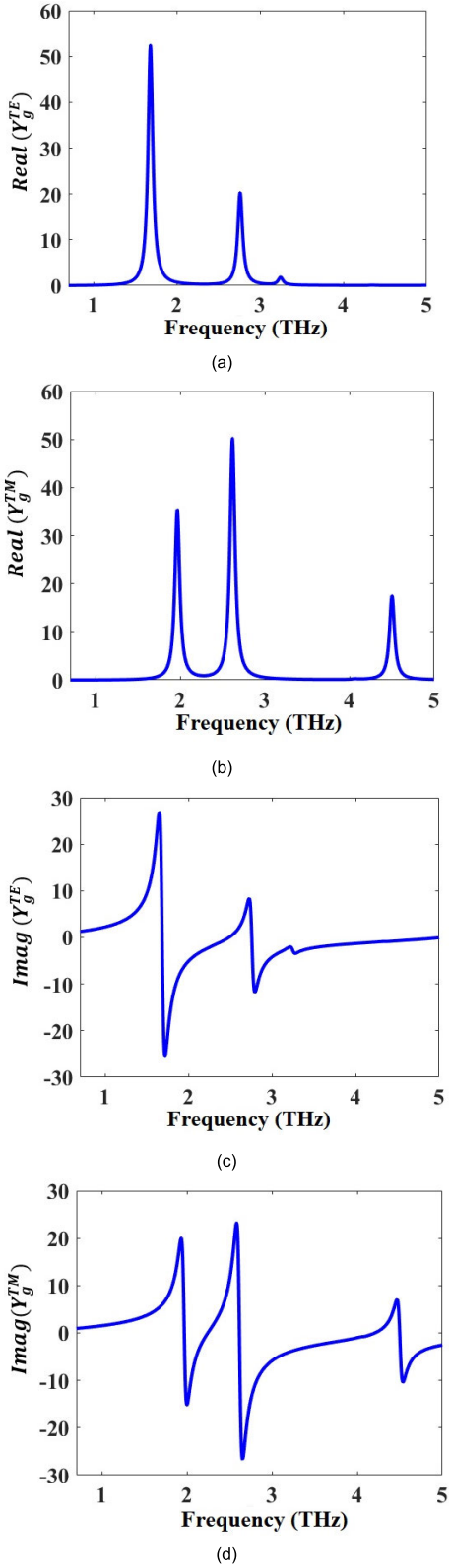

FIGURE 4. The real parts of (a) $Y_g^{TE}(\omega, \theta_{in})$ (Eq. 16), (b) $Y_g^{TM}(\omega, \theta_{in})$ (Eq. 17), the imaginary parts of (c)$Y_g^{TE}(\omega, \theta_{in})$ (Eq. 16), and (d) $Y_g^{TM}(\omega, \theta_{in})$ (Eq. 17).

So:

$$Y_{ig}^{TE} = Y_0\sqrt{\varepsilon_{ig}}\sec\left(\theta_{ig}\right) \tag{23}$$

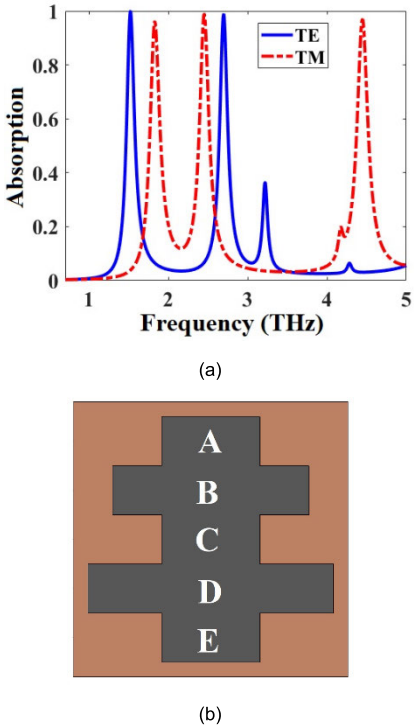

FIGURE 5. (a) Absorption spectra of the designed graphene absorber of Fig. 1 for TE and TM modes. (b) Front view of the graphene resonator layer of the unit cell of the designed absorber of Fig. 1. The resonator is made of five different sections, A, B, C, D, and E.

$$Y_{ig}^{TM} = Y_0\sqrt{\varepsilon_{ig}}\cos\left(\theta_{ig}\right) \tag{24}$$

$$\beta_{dig} = \frac{\omega\sqrt{\varepsilon_{ig}}}{c} \tag{25}$$

So:

$$Y_{in}^{TE} = \frac{\left[\begin{array}{l} Y_0\sqrt{\varepsilon_{ig}}\sec\left(\theta_{ig}\right)p_2^{TE} \\ +jY_0^3\left(1+r^{TE}\right)\varepsilon_{ig}\sec^2\left(\theta_{ig}\right)\tan\left(\beta_{d_{ig}}d_{ig}\right)\end{array}\right]}{Y_0^2\left(1+r^{TE}\right)\sqrt{\varepsilon_{ig}}\sec\left(\theta_{ig}\right)+jp_2^{TE}\tan\left(\beta_{d_{ig}}d_{ig}\right)} \tag{26}$$

$$Y_{in}^{TM} = \frac{\left[\begin{array}{l} Y_0\sqrt{\varepsilon_{ig}}\cos\left(\theta_{ig}\right)p_2^{TM} \\ +jY_0^3\left(1+r^{TM}\right)\varepsilon_{ig}\cos^2\left(\theta_{ig}\right)\tan\left(\beta_{d_{ig}}d_{ig}\right)\end{array}\right]}{Y_0^2\left(1+r^{TM}\right)\sqrt{\varepsilon_{ig}}\cos\left(\theta_{ig}\right)+jp_2^{TM}\tan\left(\beta_{d_{ig}}d_{ig}\right)} \tag{27}$$

The scattering parameters in TE/TM modes (the return losses) are calculated by:

$$S_{11}^{TE} = \frac{Y_0 - Y_{in}^{TE}\cos\left(\theta_{ig}\right)}{Y_0 + Y_{in}^{TE}\cos\left(\theta_{ig}\right)} \tag{28}$$

$$S_{11}^{TM} = \frac{Y_0 - Y_{in}^{TM}\sec\left(\theta_{ig}\right)}{Y_0 + Y_{in}^{TM}\sec\left(\theta_{ig}\right)} \tag{29}$$

The reflection coefficients in TE/TM modes are calculated by:

$$R^{TE/TM} = \left|S_{11}^{TE/TM}\right|^2 \tag{30}$$

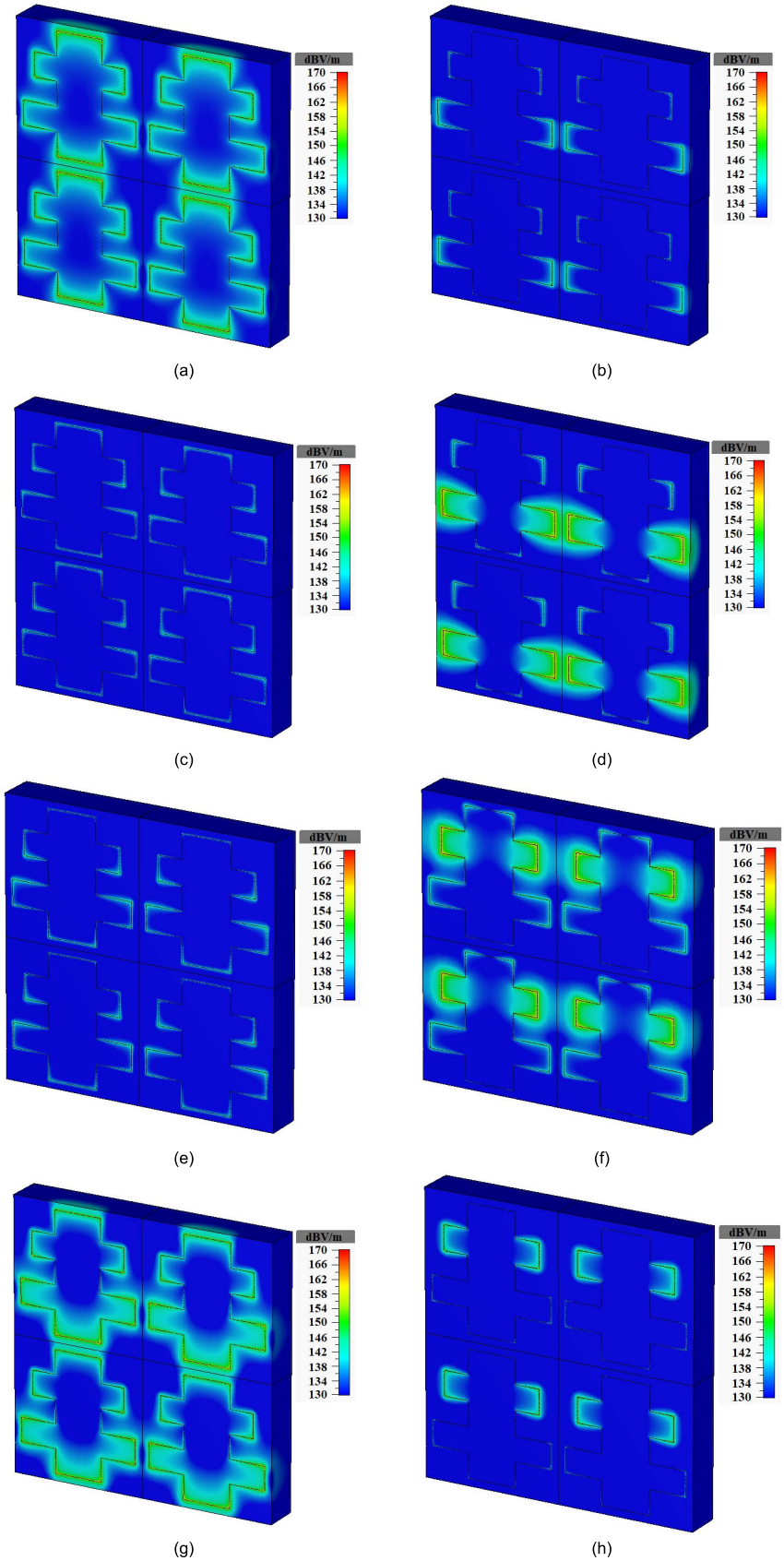

FIGURE 6. E-field distributions of the metamaterial of Fig. 1 when it is illuminated by (a) TE at 1.52 THz, (b) TM at 1.52 THz, (c) TE at 1.84 THz, (d) TM at 1.84 THz, (e) TE at 2.45 THz, (f) TM at 2.45 THz, (g) TE at 2.7 THz, (h) TM at 2.7 THz, (i) TE at 4.45 THz, and (j) TM at 4.45 THz.

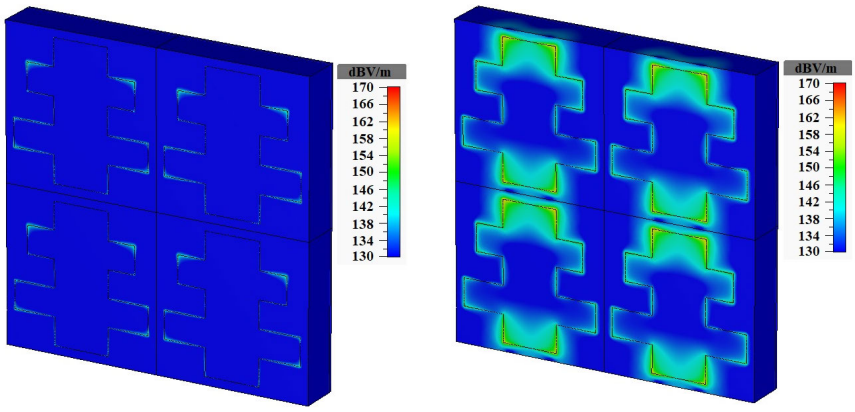

(i) (j)

FIGURE 6. *(Continued.)* **E-field distributions of the metamaterial of Fig. 1 when it is illuminated by (a) TE at 1.52 THz, (b) TM at 1.52 THz, (c) TE at 1.84 THz, (d) TM at 1.84 THz, (e) TE at 2.45 THz, (f) TM at 2.45 THz, (g) TE at 2.7 THz, (h) TM at 2.7 THz, (i) TE at 4.45 THz, and (j) TM at 4.45 THz.**

Since the metamaterial is backed by a gold reflector, there is zero transmission ($T^{TE/TM} = 0$) and the insertion losses ($S_{21}^{TE/TM}$) for TE/TM modes are zero. The absorption coefficients in TE/TM modes are calculated by:

$$A^{TE/TM} = 1 - \left|S_{11}^{TE/TM}\right|^2 = 1 - R^{TE/TM} \tag{31}$$

The linear dichroism (LD) is calculated by:

$$LD = A^{TM} - A^{TE} \tag{32}$$

III. RESULTS AND DISCUSSION

The graphene resonator array is placed on the half-space Teflon substrate with a thickness of 500 μm which is bigger than $\lambda_{max} = 428$ μm ($\lambda_{max} = c/f_{min}$ in which $f_{min} = 0.7$ THz in the 0.7-5 THz considered frequency range) to obtain the TE and TM admittances of the graphene resonator layer. The substrate is considered as a half-space to obtain the TE and TM admittances of the graphene resonator layer to avoid its influence on the TE and TM admittances of the graphene resonator layer. The configuration is simulated in CST for both TE and TM modes. The obtained reflection spectra are given in Fig. 3.

The real and the imaginary parts of the equivalent admittances (conductivities) of the graphene resonator array layer for both TE and TM modes are calculated by Eqs. 16 and 17. The obtained results are presented in Fig. 4. The graphene resonator array layer is modeled as an equivalent admittance (conductivity) which is a function of ω and θ_{in} (Fig. 2). The real parts of the equivalent admittances (conductivities) in both TE and TM modes are positive indicating the resistive nature of the graphene resonator layer representing the loss of the graphene resonator layer. In Fig. 4, it is shown that both real and imaginary parts of the equivalent admittances (conductivities) are altering in the considered frequency range which shows the graphene resonator layer is dispersive. Since the gold layer is a perfect reflector with no loss and no dispersion; and the Teflon layer has a very low loss tangent indicating a very low loss and it is assumed to be dispersionless, the main loss and dispersion are produced by graphene which causes the absorption peaks and the return loss for the metamaterial absorber. The imaginary parts of the equivalent admittances have both positive and negative parts. So, the graphene resonator layer array has both inductive and capacitive natures.

The metamaterial absorber is optimized in CST by use of the genetic algorithm to produce the lowest return loss and thus the highest absorption. The TE and TM absorption spectra of the whole graphene absorber of Fig. 1 is given in Fig. 5(a). The metamaterial absorber has two absorption bands for TE mode and three absorption bands for TM mode. Investigation of the metamaterial behavior when it is illuminated by circularly or elliptically polarized waves is not in the scope of our paper. However, if the metamaterial gets excited by circularly or elliptically polarized incident lights, then both TM and TE modes simultaneously will get excited, and the total number of absorption bands is expected to be five in these cases. The maximum absorption of each absorption band is over 96%. It has strong linear dichroism (LD) response of 98%. The average of the absorption peaks reaches 98.2%. Each of the resonators making the resonator layer array has made of five different sections: A, B, C, D, and E; as it is shown in Fig. 5(b).

The E-field distributions can also show the validity of the absorption spectra of the designed absorber for both TE and TM modes. In each resonance, the E-field distributions are not equal for TE and TM modes. For each resonance, the metamaterial only resonates in one of the TE and TM modes. The E-field distributions of the multi-band graphene absorber of Fig. 1 at 1.52 THz for TE and TM modes are respectively shown in Figs. 6(a) and 6(b). The resonance at 1.52 THz occurs in TE mode. As it is shown in Fig. 6(a), all the borders of the graphene pattern cause the resonance in f = 1.52 THz. The E-field distributions at

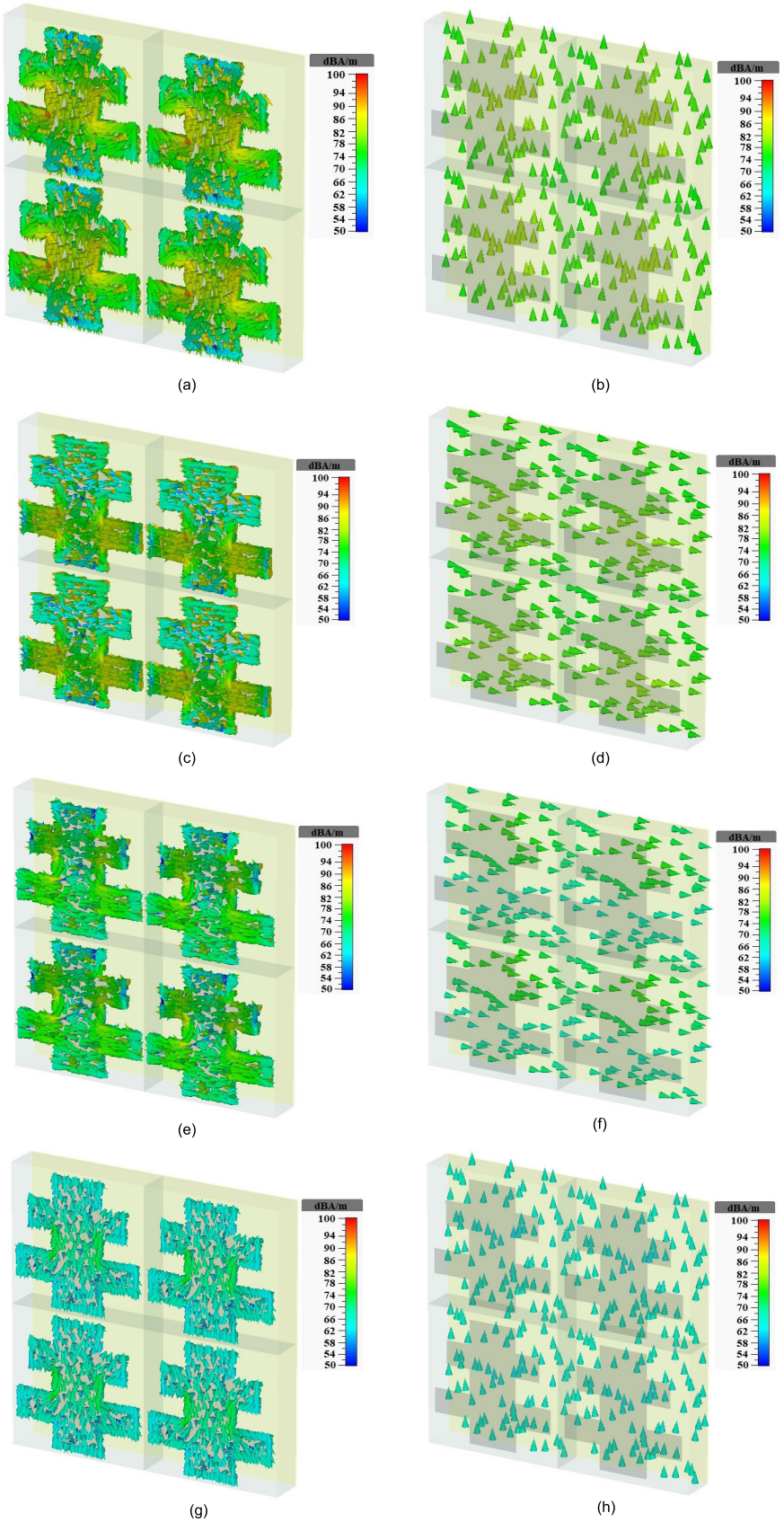

FIGURE 7. Surface current distributions of the graphene absorber of Fig. 1 at 1.52 THz on (a) graphene resonator layer, (b) gold layer, at 1.84 THz on (c) graphene resonator layer, (d) gold layer, at 2.45 THz on (e) graphene resonator layer, (f) gold layer, at 2.7 THz on (g) graphene resonator layer, (h) gold layer, at 4.45 THz on (i) graphene resonator layer, and (j) gold layer.

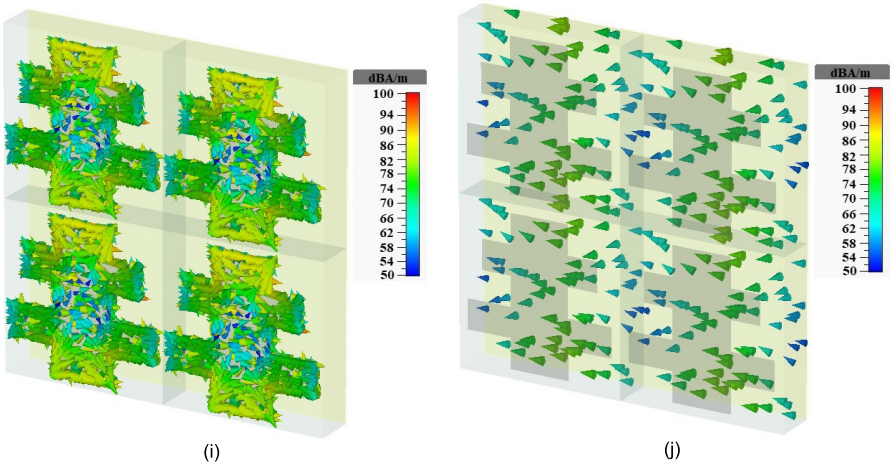

FIGURE 7. *(Continued.)* **Surface current distributions of the graphene absorber of Fig. 1 at 1.52 THz on (a) graphene resonator layer, (b) gold layer, at 1.84 THz on (c) graphene resonator layer, (d) gold layer, at 2.45 THz on (e) graphene resonator layer, (f) gold layer, at 2.7 THz on (g) graphene resonator layer, (h) gold layer, at 4.45 THz on (i) graphene resonator layer, and (j) gold layer.**

1.84 THz are given in Figs. 6(c) and 6(d). The resonance at 1.84 THz occurs in TM mode. As it is shown in Fig. 6(d), the borders of the D zone of the graphene pattern cause the resonance in f = 1.84 THz. The E-field distributions at 2.45 THz are given in Figs. 6(e) and 6(f). The resonance at 2.45 THz occurs in TM mode. As it is shown in Fig. 6(f), the borders of the B zone of the graphene pattern cause the resonance in f = 2.45 THz. The E-field distributions at 2.7 THz are given in Figs. 6(g) and 6(h). The resonance at 2.7 THz occurs in TE mode. As it is shown in Fig. 6(g), all the borders of the graphene pattern cause the resonance in f = 2.7 THz. The E-field distributions at 4.45 THz are given in Figs. 6(i) and 6(j). The resonance at 4.45 THz occurs in TM mode. As it is shown in Fig. 6(j), the borders of the A and E zones of the graphene pattern cause the resonance in f = 4.45 THz.

The surface current distributions in each resonance are also given in Fig. 7 to determine the type of the resonances (electric or magnetic). The surface currents at 1.52 THz in TE mode for the graphene resonator array and the metal gold back layer are respectively given in Figs. 7(a) and 7(b). Considering all borders of the graphene pattern (based on Fig. 6(a)), the surface currents on the pattern are up to down. The surface currents on the gold layer are down to up. The resonance is magnetic type. The surface currents at 1.84 THz in TM mode for the graphene resonator array and the gold layer are respectively given in Figs. 7(c) and 7(d). Considering the D zone of the graphene pattern (based on Fig. 6(d)), the surface currents on the D zone of the pattern are right to left. The surface currents on the gold layer are left to right. The resonance is magnetic type. The surface currents at 2.45 THz in TM mode for the graphene resonator array and the gold layer are respectively given in Figs. 7(e) and 7(f). Considering the B zone of the graphene pattern (based on Fig. 6(f)), the surface currents on the B zone of the pattern are right to left. The surface currents on the gold layer are left to right. The resonance is magnetic type. The surface currents at 2.7 THz in TE mode for the graphene resonator array and the gold layer are respectively given in Figs. 7(g) and 7(h). Considering all borders of the graphene pattern (based on Fig. 6(g)), the surface currents on the pattern are down to up. The surface currents on the gold layer are down to up. The resonance is electric type. The surface currents at 4.45 THz in TM mode for the graphene resonator array and the gold layer are respectively given in Figs. 7(i) and 7(j). Considering the A and E zones of the graphene pattern (based on Fig. 6(j)), the surface currents on these zones of the pattern are left to right. The surface currents on the gold layer are right to left. The resonance is magnetic type.

The linear dichroism (LD) vs frequency spectra of the designed graphene absorber of Fig. 1 for three different chemical potentials are calculated by Eq. 32 and the results are given in Fig. 8(a). The maximum of LD reaches 98%. By increasing of the graphene chemical potential, the resonance frequencies of the LD spectra increase, showing a blueshift. This is because the real part of the β in Eq. 4 decreases as the chemical potential increases [59]. So, the resonances increase by the increase of the chemical potential.

The linear dichroism (LD) vs frequency spectra of the designed graphene absorber of Fig. 1 for three different angles of the incident launched wave are given in Fig. 8(b). As it is shown, changing the incident wave angle affects the resonance frequencies of the LD spectrum and the LD values very slightly. So, the metamaterial is incident angle independent.

TE and TM absorption spectra of the graphene absorber of Fig. 1 with both CST and ECM approaches are obtained and given in Fig. 9. The results obtained with both methods are in good agreement.

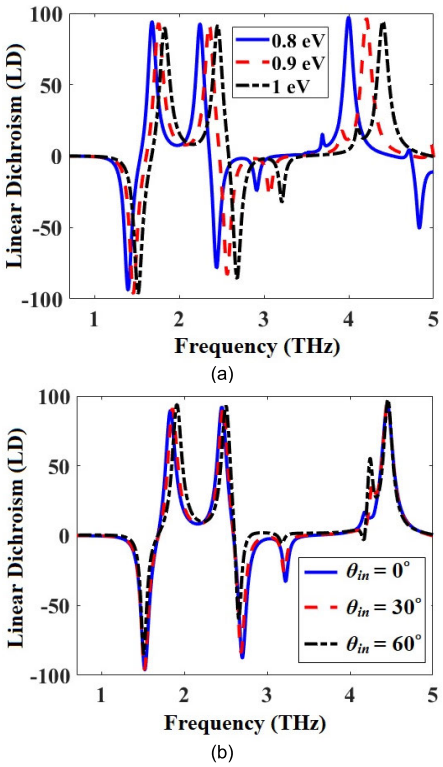

FIGURE 8. Linear dichroism (LD) vs frequency for three different values of (a) μ_c and (b) θ_{in}.

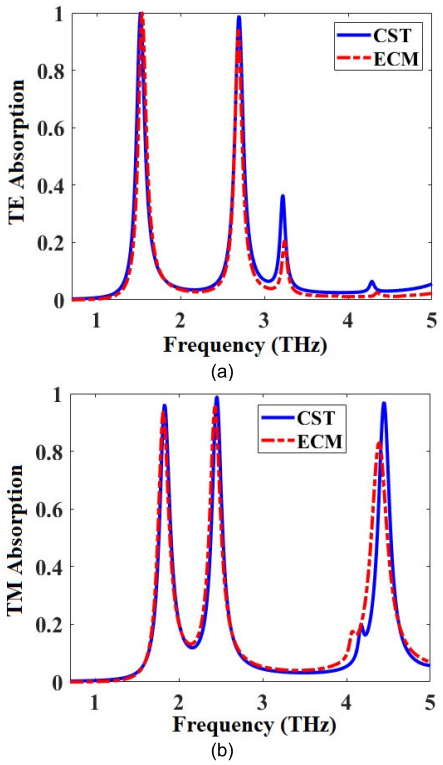

FIGURE 9. Comparison of CST and equivalent circuit modeling (ECM) absorption spectra for the graphene absorber of Fig. 1 in (a) TE and (b) TM modes.

The fabrication procedure of the device may be considered by the future readers of the work since the numerical simulation and circuit modeling is in the scope of this paper. The fabrication procedure needs further investigation, but it can be done and followed as: The Teflon dielectric is transferred on gold metal reflector through thermal evaporation. The graphene layer is coated on the Teflon dielectric by chemical vapor deposition (CVD). The double-sided graphene comb resonator array is written by electron beam etching. The ion gel dielectric is transferred on graphene resonator array through thermal evaporation [33], [60], [61].

Our designed absorber is compared with some previously published absorbers containing non-symmetrical geometries in Table 2.

TABLE 2. Comparison of the designed absorber with some previously published absorbers containing non-symmetrical geometries.

Ref.	Tunability	Frequency range	Max. absorption (%)	Max. chirality response (%)	Max. number of absorption bands
[12]	yes	1–5.5 THz	100	99	three
[27]	no	7–10 GHz	93.2	86	one
[28]	no	375–500 THz	80	50	one
[29]	no	187.5–375 THz	50	12	two
[30]	no	1.6–3.2 THz	97	70	one
[32]	no	150–250 THz	85	50	one
[33]	yes	0.5–4.5 THz	99	94	three
This work	**yes**	**0.7–5 THz**	**100**	**98**	**three**

IV. CONCLUSION

In this work, equivalent circuit modeling (ECM) approach based on admittance by using a simple MATLAB code for a terahertz (THz) graphene absorber consisted of a non-symmetric double-sided comb resonator array is designed and presented. The admittance-based ECM could be utilized for any metamaterial absorber containing one layer of resonators sandwiched between two dielectric slabs and backed by a metal layer, consisting of a layer of resonators with a thickness much smaller than the minimum wavelength in the considered wavelength range. The metamaterial is numerically simulated in CST Microwave Studio Software by use of finite element method (FEM). FEM and ECM results are in good agreement. The designed ECM can also be utilized for modeling of other graphene metamaterials containing one layer of resonator array. The designed absorber is dynamically tunable, consisting of one-layer resonator array, one resonator for each unit cell. The metamaterial absorber has a strong linear dichroism (LD) response of 98%. The absorption for all the five resonance bands is >96% and the average of the absorption peaks reaches 98.2%. The metamaterial absorber has two absorption bands for TE mode and three absorption bands for TM mode. Our designed graphene absorber can be used as an element in

controllable polarization-sensitive systems for absorbing and sensing applications.

CONFLICT OF INTEREST

None of the authors have a conflict of interest to disclose.

REFERENCES

[1] J. Liu, Z. Li, W. Liu, H. Cheng, S. Chen, and J. Tian, "High-efficiency mutual dual-band asymmetric transmission of circularly polarized waves with few-layer anisotropic metasurfaces," *Adv. Opt. Mater.*, vol. 4, no. 12, pp. 2028–2034, Dec. 2016.

[2] E. Plum, V. A. Fedotov, and N. I. Zheludev, "Optical activity in extrinsically chiral metamaterial," *Appl. Phys. Lett.*, vol. 93, no. 19, Nov. 2008, Art. no. 191911.

[3] Z. Liang, P. Liu, Z. Lin, X. Zhang, Z. Zhang, and Y.-S. Lin, "Electromagnetic responses of symmetrical and asymmetrical infrared ellipse-shape metamaterials," *OSA Continuum*, vol. 2, no. 7, pp. 2153–2161, Jul. 2019.

[4] J. Li, J. Fu, Q. Liao, and S. Ke, "Exceptional points in chiral metasurface based on graphene strip arrays," *J. Opt. Soc. Amer. B, Opt. Phys.*, vol. 36, no. 9, pp. 2492–2498, Sep. 2019.

[5] J. Li, C. Zheng, J. Li, H. Zhao, X. Hao, H. Xu, Z. Yue, Y. Zhang, and J. Yao, "Polarization-dependent and tunable absorption of terahertz waves based on anisotropic metasurfaces," *Opt. Exp.*, vol. 29, no. 3, pp. 3284–3295, Feb. 2021.

[6] J. Xu, J. Tang, M. Chen, C. Teng, S. Deng, Y. Cheng, S. Qu, and L. Yuan, "Actively tunable linear and circular dichroic metamirrors based on single-layer graphene," *Opt. Exp.*, vol. 31, no. 1, pp. 381–395, Jan. 2023.

[7] B. Sun and Y. Yu, "Analysis of circular dichroism in chiral metamaterial at terahertz frequencies," *J. Phys. D, Appl. Phys.*, vol. 52, no. 2, Nov. 2018, Art. no. 025105.

[8] L. Wang, X. Huang, M. Li, and J. Dong, "Chirality selective metamaterial absorber with dual bands," *Opt. Exp.*, vol. 27, no. 18, pp. 25983–25993, Sep. 2019.

[9] L. Mao, K. Liu, S. Zhang, and T. Cao, "Extrinsically 2D-chiral metamirror in near-infrared region," *ACS Photon.*, vol. 7, no. 2, pp. 375–383, Feb. 2020.

[10] R. R. Jones, C. Miksch, H. Kwon, C. Pothoven, K. R. Rusimova, M. Kamp, K. Gong, L. Zhang, T. Batten, B. Smith, A. V. Silhanek, P. Fischer, D. Wolverson, and V. K. Valev, "Dense arrays of nanohelices: Raman scattering from achiral molecules reveals the near-field enhancements at chiral metasurfaces," *Adv. Mater.*, vol. 10, Feb. 2023, Art. no. 2209282.

[11] Z. Yang, Z. S. Jing, Q. Y. Su, G. W. Qin, and Z. L. Zhou, "Design, simulation and experiment of polarization transformers based on twisted chiral metamaterials," *Adv. Mater. Res.*, vols. 989–994, pp. 1196–1199, Jul. 2014.

[12] S. Asgari and T. Fabritius, "Graphene-based multiband chiral metamaterial absorbers comprised of square split-ring resonator arrays with different numbers of gaps, and their equivalent circuit model," *IEEE Access*, vol. 10, pp. 63658–63671, 2022.

[13] T. Lu, D. Zhang, P. Qiu, J. Lian, M. Jing, B. Yu, J. Wen, and S. Zhuang, "Dual-band perfect metamaterial absorber based on an asymmetric H-shaped structure for terahertz waves," *Materials*, vol. 11, no. 11, p. 2193, Nov. 2018.

[14] Z. Y. Wang, Z. X. Geng, and W. H. Fang, "Exploring performance of THz metamaterial biosensor based on flexible thin-film," *Opt. Exp.*, vol. 28, no. 18, pp. 26370–26384, Aug. 2020.

[15] M. Zhang, D. Hao, S. Wang, R. Li, S. Wang, Y. Ma, R. Moro, and L. Ma, "Chiral biosensing using terahertz twisted chiral metamaterial," *Opt. Exp.*, vol. 30, no. 9, pp. 14651–14660, Apr. 2022.

[16] B. Lemkalli, M. Kadic, Y. E. Badri, S. Guenneau, A. Mir, and Y. Achaoui, "Longitudinal-twist wave converter based on chiral metamaterials," *Appl. Phys.*, vol. 10, Nov. 2022, Art. no. 48550.

[17] Z. Chen, X. Chen, L. Tao, K. Chen, R. Zhang, M. Long, E. Pickwell-MacPherson, and J. Xu, "Broadband graphene-based electro-optic chiral polarization conversion for terahertz pulse shaping," *ACS Photon.*, vol. 9, no. 11, pp. 3633–3641, Oct. 2022.

[18] E. Azmoudeh and S. Farazi, "Ultrafast and low power all-optical switching in the mid-infrared region based on nonlinear highly doped semiconductor hyperbolic metamaterials," *Opt. Exp.*, vol. 29, no. 9, pp. 13504–13517, Apr. 2021.

[19] W.-T. Gao, C. Yang, Y.-T. Tan, and J. Ren, "Reversible topological non-reciprocity by positive–negative Poisson's ratio switch in chiral metamaterials," *Appl. Phys. Lett.*, vol. 121, no. 7, Aug. 2022, Art. no. 071702.

[20] S. Asgari and T. Fabritius, "Graphene-based dual-functional chiral metamirror composed of complementary 90° rotated U-shaped resonator arrays and its equivalent circuit model," *Sci. Rep.*, vol. 11, no. 1, p. 23827, Dec. 2021.

[21] P. Kumar, A. Lakhtakia, and P. K. Jain, "Graphene pixel-based polarization-insensitive metasurface for almost perfect and wideband terahertz absorption," *J. Opt. Soc. Amer. B, Opt. Phys.*, vol. 36, no. 8, pp. F84–F88, 2019.

[22] G. C. Park and K. Park, "Tunable dual-wavelength absorption switch with graphene based on an asymmetric guided-mode resonance structure," *Opt. Exp.*, vol. 29, no. 5, pp. 7307–7320, Mar. 2021.

[23] F. Bonaccorso, Z. Sun, T. Hasan, and A. C. Ferrari, "Graphene photonics and optoelectronics," *Nature Photon.*, vol. 4, no. 9, pp. 611–622, Sep. 2010.

[24] M. Esfandiari, A. Lalbakhsh, P. N. Shehni, S. Jarchi, M. Ghaffari-Miab, H. N. Mahtaj, S. Reisenfeld, M. Alibakhshikenari, S. Koziel, and S. Szczepanski, "Recent and emerging applications of graphene-based metamaterials in electromagnetics," *Mater. Des.*, vol. 221, Sep. 2022, Art. no. 110920.

[25] S. Roy, S. Mondal, and K. Debnath, "Graphene-based chiral metasurface for generation of tunable circular dichroism—Design and sensor applications," *IEEE Sensors J.*, vol. 23, no. 1, pp. 285–292, Jan. 2023.

[26] H. Li, J. Li, C. Zheng, H. Xu, F. Yang, J. Li, Z. Yue, W. Shi, Y. Zhang, and J. Yao, "Dual-band giant spin-selective full-dimensional manipulation of graphene-based chiral meta-mirrors for terahertz waves," *Opt. Exp.*, vol. 30, no. 12, pp. 22292–22305, Jun. 2022.

[27] M. Li, L. Guo, J. Dong, and H. Yang, "An ultra-thin chiral metamaterial absorber with high selectivity for LCP and RCP waves," *J. Phys. D, Appl. Phys.*, vol. 47, no. 18, Apr. 2014, Art. no. 185102.

[28] B. Tang, Z. Li, E. Palacios, Z. Liu, S. Butun, and K. Aydin, "Chiral-selective plasmonic metasurface absorbers operating at visible frequencies," *IEEE Photon. Technol. Lett.*, vol. 29, no. 3, pp. 295–298, Feb. 1, 2017.

[29] X.-T. Kong, L. K. Khorashad, Z. Wang, and A. O. Govorov, "Photothermal circular dichroism induced by plasmon resonances in chiral metamaterial absorbers and bolometers," *Nano Lett.*, vol. 18, no. 3, pp. 2001–2008, Feb. 2018.

[30] Y. Cheng, H. Chen, J. Zhao, X. Mao, and Z. Cheng, "Chiral metamaterial absorber with high selectivity for terahertz circular polarization waves," *Opt. Mater. Exp.*, vol. 8, no. 5, pp. 1399–1409, May 2018.

[31] X. Yang, M. Li, Y. Hou, J. Du, and F. Gao, "Active perfect absorber based on planar anisotropic chiral metamaterials," *Opt. Exp.*, vol. 27, no. 5, pp. 6801–6814, Mar. 2019.

[32] L. Ouyang, D. Rosenmann, D. A. Czaplewski, J. Gao, and X. Yang, "Broadband infrared circular dichroism in chiral metasurface absorbers," *Nanotechnology*, vol. 31, no. 29, May 2020, Art. no. 295203.

[33] S. Asgari and T. Fabritius, "Equivalent circuit model of graphene chiral multi-band metadevice absorber composed of U-shaped resonator array," *Opt. Exp.*, vol. 28, no. 26, pp. 39850–39867, Dec. 2020.

[34] H. S. Singh, "Super compact ultrathin quad-band with wide angle stability polarization independent metamaterial absorber," *Microw. Opt. Technol. Lett.*, vol. 62, no. 2, pp. 718–725, Oct. 2019.

[35] Y. Liu, R. Zhong, J. Huang, Y. Lv, C. Han, and S. Liu, "Independently tunable multi-band and ultra-wide-band absorbers based on multilayer metal-graphene metamaterials," *Opt. Exp.*, vol. 27, no. 5, pp. 7393–7404, Mar. 2019.

[36] Y. He, Q. Wu, and S. Yan, "Multi-band terahertz absorber at 0.1–1 THz frequency based on ultra-thin metamaterial," *Plasmonics*, vol. 14, no. 6, pp. 1303–1310, Mar. 2019.

[37] K.-D. Xu, J. Li, A. Zhang, and Q. Chen, "Tunable multi-band terahertz absorber using a single-layer square graphene ring structure with T-shaped graphene strips," *Opt. Exp.*, vol. 28, no. 8, pp. 11482–11492, Apr. 2020.

[38] Z. Yi, J. Huang, C. Cen, X. Chen, Z. Zhou, Y. Tang, B. Wang, Y. Yi, J. Wang, and P. Wu, "Nanoribbon-ring cross perfect metamaterial graphene multi-band absorber in THz range and the sensing application," *Results Phys.*, vol. 14, Sep. 2019, Art. no. 102367.

[39] S. Barzegar-Parizi and A. Ebrahimi, "Ultrathin, polarization-insensitive multi-band absorbers based on graphene metasurface with THz sensing application," *J. Opt. Soc. Amer. B, Opt. Phys.*, vol. 37, no. 8, pp. 2372–2381, 2020.

[40] Q. Zhou, P. Liu, L.-A. Bian, X. Cai, and H. Liu, "Multi-band terahertz absorber exploiting graphene metamaterial," *Opt. Mat. Exp.*, vol. 8, no. 9, pp. 2928–2940, Sep. 2018.
[41] P. Jain, S. Bansal, K. Prakash, N. Sardana, N. Gupta, S. Kumar, and A. K. Singh, "Graphene-based tunable multi-band metamaterial polarization-insensitive absorber for terahertz applications," *J. Mater. Sci., Mater. Electron.*, vol. 31, no. 14, pp. 11878–11886, Jul. 2020.
[42] Z. Wu, J. Tian, and R. Yang, "A graphene based dual-band metamaterial absorber for TE polarized THz wave," *Micro Nanostruct.*, vol. 168, Aug. 2022, Art. no. 207331.
[43] T. Aghaee and A. A. Orouji, "Reconfigurable multi-band, graphene-based THz absorber: Circuit model approach," *Results Phys.*, vol. 16, Mar. 2020, Art. no. 102855.
[44] N. Matthaiakakis, X. Yan, H. Mizuta, and M. D. B. Charlton, "Tuneable strong optical absorption in a graphene-insulator-metal hybrid plasmonic device," *Sci. Rep.*, vol. 7, no. 1, p. 7303, Aug. 2017.
[45] A. Kamarauskas, D. Seliuta, G. Šlekas, M. Sadauskas, E. Kvietkauskas, R. Trusovas, K. Ratautas, and Ž. Kancleris, "Experimental demonstration of multiple Fano resonances in a mirrored array of split-ring resonators on a thick substrate," *Sci. Rep.*, vol. 12, no. 1, p. 15846, Sep. 2022.
[46] S. Rajesh, V. S. Nisa, K. P. Murali, and R. Ratheesh, "Microwave dielectric properties of PTFE/rutile nanocomposites," *J. Alloys Compounds*, vol. 477, nos. 1–2, pp. 677–682, May 2009.
[47] Q. Zhou, S. Zha, P. Liu, C. Liu, L.-A. Bian, J. Zhang, H. Liu, and L. Ding, "Graphene based controllable broadband terahertz metamaterial absorber with transmission band," *Materials*, vol. 11, no. 12, p. 2409, Nov. 2018.
[48] G. Yao, F. Ling, J. Yue, C. Luo, J. Ji, and J. Yao, "Dual-band tunable perfect metamaterial absorber in the THz range," *Opt Exp.*, vol. 24, no. 2, pp. 1518–1527, Jan. 2016.
[49] M. Biabanifard, S. Asgari, S. Biabanifard, and M. S. Abrishamian, "Analytical design of tunable multi-band terahertz absorber composed of graphene disks," *Optik*, vol. 182, pp. 433–442, Apr. 2019.
[50] M. Islam, S. J. M. Rao, G. Kumar, B. P. Pal, and D. Roy Chowdhury, "Role of resonance modes on terahertz metamaterials based thin film sensors," *Sci. Rep.*, vol. 7, no. 1, p. 7355, Aug. 2017.
[51] R. Sarkar, D. Ghindani, K. M. Devi, S. S. Prabhu, A. Ahmad, and G. Kumar, "Independently tunable electromagnetically induced transparency effect and dispersion in a multi-band terahertz metamaterial," *Sci. Rep.*, vol. 9, no. 1, p. 18068, Dec. 2019.
[52] J. McCall, "Genetic algorithms for modelling and optimisation," *J. Comput. Appl. Math.*, vol. 184, no. 1, pp. 205–222, Dec. 2005.
[53] S. Asgari, E. Shokati, and N. Granpayeh, "High-efficiency tunable plasmonically induced transparency-like effect in metasurfaces composed of graphene nano-rings and ribbon arrays and its application," *Appl. Opt.*, vol. 58, no. 13, pp. 3664–3670, 2019.
[54] M. Rahmanzadeh, A. Khavasi, and B. Rejaei, "Analytical method for the diffraction of an electromagnetic wave by subwavelength graphene ribbons," *J. Opt. Soc. Amer. B, Opt. Phys.*, vol. 38, no. 3, pp. 953–960, 2021.
[55] M. Rahmanzadeh, A. Khavasi, and B. Rejaei, "Analytical method for diffraction analysis and design of perfect-electric-conductor backed graphene ribbon metagratings," *Opt. Exp.*, vol. 29, no. 18, pp. 28935–28952, Aug. 2021.
[56] B. Wang, X. Zhang, X. Yuan, and J. Teng, "Optical coupling of surface plasmons between graphene sheets," *Appl. Phys. Lett.*, vol. 100, no. 13, Mar. 2012, Art. no. 131111.
[57] D. K. Cheng, *Field and Wave Electromagnetics*. Chennai, India: Pearson, 1989.
[58] A. Andryieuski and A. V. Lavrinenko, "Graphene metamaterials based tunable terahertz absorber: Effective surface conductivity approach," *Opt. Exp.*, vol. 21, no. 7, pp. 9144–9155, Apr. 2013.
[59] S. Asgari, N. Granpayeh, and T. Fabritius, "Controllable terahertz cross-shaped three-dimensional graphene intrinsically chiral metastructure and its biosensing application," *Opt. Commun.*, vol. 474, Nov. 2020, Art. no. 126080.
[60] Z. Yi, C. Liang, X. Chen, Z. Zhou, Y. Tang, X. Ye, Y. Yi, J. Wang, and P. Wu, "Dual-band plasmonic perfect absorber based on graphene metamaterials for refractive index sensing application," *Micromachines*, vol. 10, no. 7, p. 443, Jul. 2019.
[61] B. G. Ghamsari, A. Olivieri, F. Variola, and P. Berini, "Enhanced Raman scattering in graphene by plasmonic resonant Stokes emission," *Nanophotonics*, vol. 3, no. 6, pp. 363–371, Dec. 2014.

SOMAYYEH ASGARI received the B.Sc. degree in electrical and power electronics engineering from the University of Zanjan, Zanjan, Iran, in 2014, and the M.Sc. degree in telecommunication engineering from the K. N. Toosi University of Technology, Tehran, Iran, in 2017. She is currently pursuing the Ph.D. degree with the Optoelectronics and Measurement Techniques Research Unit, Faculty of Information Technology and Electrical Engineering, University of Oulu, Oulu, Finland. She is the author and coauthor of 25 peer-reviewed journal and three conference papers. Her research interests include the design and simulation of solar cells, optical metamaterials, chiral metastructures, graphene plasmonic devices and structures, MEMS metamaterials, and linear and nonlinear plasmonic metal-based devices.

TAPIO FABRITIUS received the M.Sc. and D.Sc. degrees in applied electronics engineering from the University of Oulu, Oulu, Finland, in 2003 and 2007, respectively. Since 2003, he has been with the University of Oulu, where he is currently a Full Professor and the Head of the Optoelectronics and Measurement Techniques Research Unit. He has authored over 135 peer-reviewed journal and conference papers. His current research interests include the development of instrumentation and printed intelligence manufacturing technologies and metamaterials.